Bond graph models of DC-DC converters operating in both CCM and DCM

Article

Accepted Version

Bond Graph Models of DC-DC Converters Operating in Both CCM and DCM

Antonios Markakis, William Holderbaum, Ben Potter

April 28,2014

Abstract

In this paper, Bond Graphs are employed to develop a novel mathematical model of conventional switched-mode DC-DC converters valid for both continuous and discontinuous conduction modes. A unique causality bond graph model of hybrid models is suggested with the operation of the switch and the diode to be represented by a Modulated Transformer with a binary input and a resistor with fixed conductance causality. The operation of the diode is controlled using an if-then function within the model. The extracted hybrid model is implemented on a Boost and Buck converter with their operations to change from CCM to DCM and to return to CCM. The vector fields of the models show validity in a wide operation area and comparison with the simulation of the converters using PSPICE reveals high accuracy of the proposed model, with the Normalised Root Means Square Error and the Maximum Absolute Error remaining adequately low. The model is also experimentally tested on a Buck topology.

1 Introduction

In most applications a DC-DC power converter will be designed to operate in either Continuous Conduction Mode (CCM) or Discontinuous Conduction Mode (DCM), and the model for converter would be different in each case. However, there are applications where the converters are required to operate in the boundaries of the two operation modes, like the Interleaved DCM/CCM Boundary Power Factor Correction (PFC) Converters (Lai & Chen 1993, Huber et al. 2008) or converters where their load or their switching frequency changes significantly during operation allowing them to pass from one mode to the other. In such cases, two models are derived and two different controls are implemented; the transition between CCM and DCM must be detected and the correct model and controller selected. For one converter with n storage elements capable of passing from CCM to DCM the number of the models that need to be derived is given by $k = 2^n$, and as a result $d = n \cdot k$ different differential equations need to be derived. The complexity increases exponentially for a system of more than one converter.

A conventional approach to model a converter that passes from CCM to DCM is to derive the averaged model for both CCM and the DCM through a State Space Averaging (SSA) technique (Middlebrook & Cuk 1977). However, using the SSA method results in inaccuracies in the final models as well as in difficulties with calculations (Moussa & Morris 1990). Moreover, using the SSA technique, the diode is assumed to be a switch which operates complementary with the main switch of the converter. In DCM, complementary switching is not adequate to define the operation of the converter as within one period an additional time interval exists when the one of the state variables reaches and remains at zero. A volt-second balance is employed to define this time interval but the model appears with a reduced order (Cuk & Middlebrook 1977). A solution has been suggested by Mitchell et al. (2001) although the obtained mathematical model is more complicated.

The PWM-Switch Modelling Method was suggested by Vorperian (1990*b*,*a*). This method uses the concept of a fictitious Single-Pole-Double-Throw (SPDT) switch to represent the operation of the switch and the diode. Furthermore, Femia & Tucci (1994) present an approach that uses a fictitious switch to represent both CCM and DCM. This method gives more accurate results than State-Space Averaging since linearisation happens only in the non-linear part responsible for the switching, whereas the entire system is linearised in SSA. However, as with SSA, the implementation of the PWM-Switch Modelling method is based on the assumption that the switch and the diode operate complementary. Finally, both methods produce the

averaged values of the state variables, which has an impact in the accuracy of the models that are developed. The focus of this paper is the development of a modelling method for CCM and DCM operation of DC-DC converters that does not assume complementary operation of the switches, does not linearise across the whole system and does not average the state variables. The central tool to develop such a model is Bond Graphs.

Bond Graphs (Paynter & Briggs 1961, Rai & Umanand 2009) is a Mechatronics modelling technique utilised to model interconnected interacting physical systems. Bond Graphs have been designed to represent the continuous flow of the power or the energy exchanges within the components of a system. Hence, abrupt changes on that flow, like the operation of a common switch in Hybrid Systems, can not be directly represented without modifications to the method. Systems are defined as hybrid, when they contain both continuous states as well as discrete phenomena (Mirzaei & Afzalian 2009). Throughout the years, several methods have been suggested and reviewed for representing hybrid systems using Bond Graphs. As mentioned by Mosterman & Biswas (1998), the modelling of Hybrid Systems using Bond Graphs creates two sub categories: models with causalities that remain unchanged during commutation (fixed causalities) and their variables do not depend upon the ON-OFF mode of a switch, and models with variable causalities where the integral causality changes during commutation.

A comparison between Bond Graph modelling methods which lead to fixed causalities and those with variable causalities is presented by Mosterman & Biswas (1998), Dauphin-Tanguy & Rombaut (1993), Borutzky (1995), Buisson et al. (2002), Umarikar & Umanand (2005*b*,*a*), Markakis et al. (2011). In Mosterman & Biswas (1998) and Markakis et al. (2011) Bond Graph models with variable causalities are used for each switching mode. However, this approach results in a disadvantage. For systems containing more than one switches, the number of configurations required to be calculated is up to n^k, where n is the number of switching components and k is the behaviour modes of each component. Therefore, for converters containing a switch with two modes (on, off) k is equal to $k = 2$. Particularly for the *"Ideal Switch Element"* method, an additional resistive element is suggested to be used in order for the causality to remain the same across the storage elements although the causality changes in this additional resistive elements during the commutation (Buisson 1993). The same method for the representation of a switch has been proposed by Buisson (2001) but this technique is valid only when the switches operate complementary.

In this paper, a combination of a Modulated Transformer with a binary modulation ratio and a resistor (MTF-R method) is employed to represent the operation of a switch. This method has been proposed by Dauphin-Tanguy & Rombaut (1993), Ducreux et al. (1993), Borutzky (1995, 2010, 2012) and leads to a fixed causality bond graph model. Consequently, the resulting model is not segmented according to the state of the switch. Additionally, this method allows the modelling of several switches within a network without requiring any correlation between them; the switches do not have to operate complementary. By permitting direct access to the on-off state of the switch, the extracted model is not the averaged model. Such a model is suitable for control strategies with direct boolean control inputs like *"Sliding Mode Control"* (Paul 2013). Finally, the operation of the diode can be represented by this method as well as will be discussed later.

The novel contribution of this paper is the use of the MTF-R method to derive a unified model valid for both CCM and DCM. The resulting model does not restricts the input, the load or the switching frequency to remain constant or within tight limits. In the following sections, the MTF-R method is demonstrated and the representation of the diode using the MTF-R method is presented. The operation of the model in both CCM and DCM is described and the validity of the obtained hybrid model is proved with a unique state space equation to be derived. The accuracy of the model is tested by its implementation on two different DC-DC converter topologies, and results are presented including the vector fields of the models and the comparison between the resulting, mathematical models and the simulation of the converters using PSPICE. Furthermore, the model is compared with the experimental results of a Buck converter. Finally, a discussion on the results follows where, the Normalised Root Means Square Error as well as the Maximum Absolute Error between the mathematical model and the simulation results is calculated.

2 Modelling of DC-DC Converter Using Bond Graphs

2.1 Modulated Transformer and Resistor to Represent the Switch Using Bond Graphs (MTF-R Method)

In this paper, the DC-DC converters are suggested to be modelled by **Bond Graphs** using the MTF-R method to model the switches. According to the MTF-R method a Bond Graph Modulated Transformer (MTF) element with Binary modulation ratio $m \in \{0, 1\}$, is combined with a resistive element R_{on} to exhibit the operation of a switching device. With reference to Fig. 1, if the modulation index of the modulated transformer is set equal to one $m = 1$, power is dissipated through the resistor R_{on}. The R_{on} value is chosen to be small and can represent the resistance of a switch when it is closed *"ON"*. In this case, the MTF-R combination provides the flow information, *f*, to the rest of the system, as it is described by the eq.(1). In electrical systems the flow, *f*, is equivalent to the current.

$$f_3 = mf_4 = m\frac{e_4}{R_{on}} = \frac{m^2}{R_{on}}e_3 \Rightarrow f_3 = \frac{m^2}{R_{on}}(e_1 - e_2) \tag{1}$$

When the modulation index of the transformer is set to be equal to zero, $m = 0$, a zero flow is implied to the rest of the system. In that case, the operation of an open switch *"OFF"* is realised, where no current is allowed to pass. The ratio $\frac{m}{R_{on}}$ shows that the conductance of the switch is high when the switch is ON and is zero when the switch is OFF. With reference to R_{on}, the causality of R_{on} remains fixed during the commutation and it is named as *"Conductance Causality.*

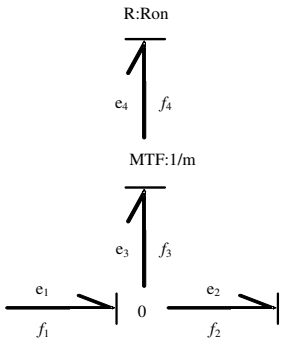

Figure 1: Bond graph model of a switch implemented by MTF - R method

2.2 The operation of a diode

For the methods described in the introduction, a diode is commonly modelled as a switch and assumed to operate complementary to the actual switch in a single-switch DC-DC converter. Such a representation may leads to erroneous models. For instance, the inductor current in a conventional DC-DC converter with one switch and one diode is restricted by the diode to remain above zero. However, the representation of a diode using a bidirectional switch model will permit the inductor current to go below zero resulting in an erroneous steady-state as well as transient response. Also, if the switch and diode are assumed to operate complementary then it will not be possible to represent DCM where the switch and diode are off for a portion of the switching cycle. The MTF-R method allows for a more accurate representation of the diode independent from the main switch. This paper uses this fundamental advantage to derive a model valid for both CCM and DCM.

A control loop external to the Bond Graphs model is established, as shown in Fig.2 (Ducreux et al. 1993, Borutzky 1995, 2010, 2012). This control loop compares the effort between the shared bonds of the diode junctions. With reference to Fig.2, when the difference of the effort, $\Delta e = e_1 - e_2$, passes a specific

threshold, e_{set}, the modulation ratio of the transformer becomes equal to one as can be tracked in eq.(2).

$$m = \begin{cases} 1 & if \quad \Delta e \geq e_{set} \\ 0 & if \quad \Delta e < e_{set} \end{cases} \tag{2}$$

The observation of the effort across the junction is internal to the system control loop. Therefore, the obtained model of Fig.2 as defined by Borutzky (2012) is a model with *Internal Modulation*. Following this definition, the flow information provided by the model of the diode to the rest of the system is a function of its flow and effort and it is not outlined by any external control.

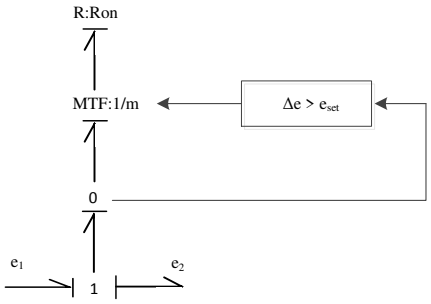

Figure 2: Bond graph model of a diode implemented by MTF - R method

The characteristics of the diode's model is presented in Fig. 3. The forward-biased part of the diode's characteristic is a line, instead of a curve, with a gradient $\frac{1}{R_{on}}$; the forward voltage drop is not represented using the MTF-R method. Nevertheless, the simulation results are affected significantly since the resulting error is very small. Also, appropriate selection of the resistor R_{on} reduces the difference between the a real diode component and the model.

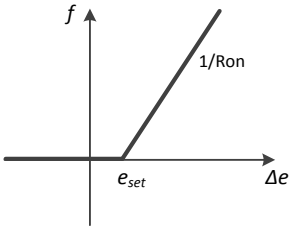

Figure 3: Static characteristic of a diode

3 Operation in CCM and DCM

In Fig. 4 an automaton diagram describes the operation of a conventional DC-DC converter and shows that the obtained model complies with this operation. In mode Σ_1 the switch is ON, $m_1 = 1$, while the diode is reversed, $m_2 = 0$. As the switch opens, $m_1 = 0$, the system passes to mode Σ_2 where the diode starts to conduct, $m_2 = 1$. There are two potential next modes depending upon the inductor's current. If the energy stored in the inductor is large enough to supply the load when the switch is OFF, the system returns to the Σ_1 and the converter operates in Continuous Conduction Mode. If the energy stored in the inductor is not enough to supply the load during the Σ_2 state, the inductor current reaches zero and the diode is reversed biased, $m_2 = 0$. At this point both the switch and the diode will not conduct, $m_1 = m_2 = 0$, and the system passes to mode Σ_3 until the switch turns ON again by the control input and the system returns to the state

Σ_1. When the system remains in the three modes $\Sigma_1, \Sigma_2, \Sigma_3$, the converter operates in DCM. The state Σ_4 describes the case where both the switch and the diode are conducting.

The novel contribution of this paper is a unified mathematical model derived from Bond Graphs for DC-DC converters operating in both CCM and DCM. In conventional DC-DC converter topologies, a switch and a diode are connected either in parallel or in series. Using Bond Graphs MTF-R method, a causality conflict occurs at the junction where the two components are connected. To solve this causality conflict an additional resistive element is added as suggested by Dauphin-Tanguy & Rombaut (1993). The causality on that additional resistor remains fixed during the commutation. This additional resistor in combination with the resistive elements of the switch and the diode does not allow the denominators of the first derivatives of the state variables to be zero when both switch and the diode are OFF, $m_1 = m_2 = 0$. Therefore, no singularity occurs in their equations when the converter operates in DCM and the extracted model has the ability to demonstrate both CCM and DCM.

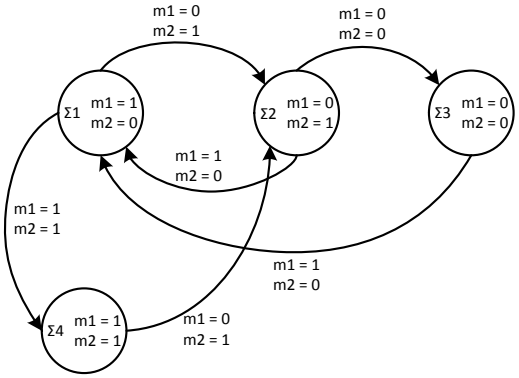

Figure 4: Automata diagram showing all the possible states of a conventional DC-DC converter

3.1 Obtained Hybrid Mathematical Model

The mathematical model of a conventional DC-DC converter obtained by the MTF-R method follows the general form of the switching Bond Graphs models as established by Buisson (2001), Buisson et al. (2002) and demonstrated in Fig. 5 The implicit formalisation is described by eq.3 (Buisson et al. 2002).

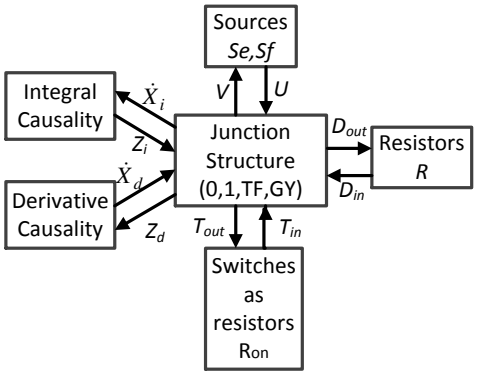

Figure 5: Block diagram describing the general structure of a switching Bond Graph model

$$\begin{bmatrix} 1 & -S_{12} \\ 0 & 0 \\ 0 & 0 \\ 0 & -S_{24}^T \\ 0 & S_{25}^T \end{bmatrix} \dot{X} = \begin{bmatrix} S_{11} & 0 & S_{13} & 0 & S_{14} & 0 & S_{15} & 0 \\ -S_{12}^T & -I & 0 & 0 & S_{24} & 0 & S_{25} & 0 \\ -S_{13}^T & 0 & S_{33} & -I & S_{34} & 0 & S_{35} & 0 \\ S_{14}^T & 0 & S_{34}^T & 0 & S_{44} & -I & S_{45} & 0 \\ S_{15}^T & 0 & S_{35}^T & 0 & S_{45} & 0 & S_{55} & -I \end{bmatrix} W \tag{3}$$

where:

$$X = \begin{bmatrix} X_i & X_d \end{bmatrix}, W = \begin{bmatrix} Z_i & Z_d & D_{in} & D_{out} & T_{in} & T_{out} & U & V \end{bmatrix}^T$$

1. - X_i denotes the state vector which consists of the energy variables in integral causality. The momentum p is for the inertia elements (inductors) I while displacement q for the complaint elements C (capacitors)
   - Z_i is the complementary state vector composed of the power variables in integral causality, e for the C elements and f for the I elements
2. - X_d named as semi-state vector which contains energy variables in derivative causality
   - Z_d is the complementary state vector in derivative causality
3. - D_{in} and D_{out} are vectors which contain the power variables going into and out of the junction structure from the resistive elements field.
4. - T_{in} and T_{out} are vectors containing the power variables going into and out of the junction structure from the switches. These variables, in variable structure systems such as the *"Ideal Switch"*, change during the commutation. Whereas in a unified representation of the switch, such as the MTF-R method, they remain invariant, f for the T_{in} and e for the T_{out}.
5. - U is the vector containing the power sources of the system
   - V is the complementary to U containing the variables provided from the system to the sources, f for the effort source *SE* and e for the flow sources *SF*.

Necessary condition for the eq.(3) is for no unit causal loops to exist. Also, due to the energy conservation on each junction, the matrices S_{11}, S_{33}, S_{44} are skew symmetric (Buisson et al. 2002).

The relation between $T_{in},\ T_{out}$ is based on eq.1 which combines the modulus of the controlled transformer with the Ohm's law. Thus, the implicit equation changes whenever the mode changes.

With the MTF-R method the causalities remain invariant and any causality conflicts are solved with additional resistive elements. Therefore, the integral causality for all the storage elements will remain during commutation. It is thus possible for the eq.(3) to be simplified by omitting the second row and column relating with derivative causality. Also, the last row of the eq.(3) corresponding to the variables provided from the system to the sources can be omitted, as it is only useful when energetic balance analysis is needed, which is out of the purposes of this paper. After implementing the above simplifications the eq.(4) results

$$\begin{bmatrix} \dot{X}_i \\ 0 \\ 0 \end{bmatrix} \begin{bmatrix} S_{11} & S_{13} & 0 & S_{14} & 0 & S_{15} \\ -S_{13}^T & S_{33} & -I & S_{34} & 0 & S_{35} \\ S_{14}^T & S_{34}^T & 0 & S_{44} & -I & S_{45} \end{bmatrix} W' \tag{4}$$

with the new $W' = \begin{bmatrix} Z_i & D_{in} & D_{out} & T_{in} & T_{out} & U \end{bmatrix}^T$

3.2 Validity of the Obtained Modes

Having established integral causality for all the storage elements, the modes described in Fig. 4 are all reference modes (Buisson et al. 2002). The eq.(5) is the criteria for these modes to be valid (Cormerais & Buisson 2000) when there is no causal path between a switch and a storage element in derivative causality $S_{24} = 0$ (Buisson et al. 2002).

$$rank\left(\Lambda\left(S_{14}^T S_{34}^T S_{44} \Lambda\right)\right) = rank\left(\Lambda\right) \tag{5}$$

where $\Lambda \in \mathbb{R}_{kxk}$ is a diagonal matrix with its elements equal to *1* when the corresponding switches change state with commutation, otherwise *0*, and k is the number of the switches (in this case $k = 2$).

When considering the operation in CCM where, the system commutates from the reference mode $\Sigma 1$ to $\Sigma 2$ and vice versa, Λ is a unity matrix and the eq.(5) is established. When $\Sigma 3$ or $\Sigma 4$ mode is involved in DCM, then λ_{11} or λ_{22} equals to zero respectively. However a reduction in the order of the system then occurs to establish the eq.(5) again. Thus, all the possible modes are valid and the operation in DCM is possible to be represented.

3.3 Unique State Space

Assuming $D_{in} = LD_{out}$, where L is a matrix consisting of the resistive values or their inverses, which depends upon the causality of the corresponding resistors. The L is symmetric if the number of the resistive elements is even. Then, the second line of the implicit equation eq.(4) can be written as:

$$L^{-1}(I - LS_{33})D_{in} = -S_{13}^T Z_i + S_{34}T_{in} + S_{35}U \tag{6}$$

The matrix $L^{-1}(I - LS_{33})$ is invertible even if a causal path between the resistive elements does not exist $S_{33} = 0$. Then the value of D_{in} is defined as:

$$D_{in} = H(-S_{13}^T Z_i + S_{34}T_{in} + S_{35}U) \tag{7}$$

where $H = L(I - S_{33}L)^{-1}$. Then, from the first line of eq.(4) and from eq.(7) the eq.(8) is established as:

$$\dot{x}_i = (S_{11} - S_{13}HS_{13}^T)Z_i + (S_{14} + S_{13}HS_{34})T_{in} + (S_{15} + S_{13}HS_{35})U \tag{8}$$

To eliminate the T_i factor from eq.(8) it is assumed that $T_{in} = E^{-1}T_{out}$ where, E is a diagonal matrix consisting of the R_{on} and the R_d values. Then the third line of the eq.(4) leads to:

$$(E - S_{44})T_{in} = S_{14}^T Z_i + S_{34}^T D_{in} + S_{45}U \tag{9}$$

The switch and the diode are connected between them and a causal path is established. However the causalities of the switch and the diode are referred to the R_{add} which results to $S_{44} = 0$. Thus, $E - S_{44} = E$ and the eq.(9) can be simplified to:

$$ET_{in} = S_{14}^T Z_i + S_{34}^T D_{in} + S_{45}U \Rightarrow T_{in} = E^{-1}(S_{14}^T Z_i + S_{34}^T D_{in} + S_{45}U) \tag{10}$$

The eq.(11) occurs from eq.(10) by substituting D_{in} from eq.(7).

$$(I - E^{-1}S_{34}^T HS_{34})T_{in} = E^{-1}(S_{14}^T - S_{34}^T HS_{13}^T)Z_i + E^{-1}(S_{34}^T HS_{35} + S_{45})U \tag{11}$$

The expression $E^{-1}S_{34}^T HS_{34} \neq I$ is always true when considering a system with one switch and one diode as the S_{34} is a non-symmetric matrix consisting of the modulation ratio of the MTF-Rs representing the switch and the diode (m_1, m_2). Moreover the matrices E^{-1}, H will always be diagonal matrices consisting of resistances. Thus $E^{-1}S_{34}^T HS_{34}$ will never be a diagonal matrix and the matrix $J = (I - E^{-1}S_{34}^T HS_{34})^{-1}$ will always exist for a network with one switch and one diode. Then, the eq.(11) is possible to be rearranged as:

$$T_{in} = JE^{-1}(S_{14}^T - S_{34}^T HS_{13}^T)Z_i + JE^{-1}(S_{34}^T HS_{35} + S_{45})U \tag{12}$$

Rearranging the fist line of the eq.(4) using the eq.(7) and the eq.(12)

$$\begin{aligned}\dot{X}_i = \{(S_{11} - S_{13}HS_{13}^T) + (S_{14} + S_{13}HS_{34})JE^{-1}(S_{14}^T - S_{34}^T HS_{13}^T)\}Z_i + \\ \{(S_{15} + S_{13}HS_{35}) + (S_{14} + S_{13}HS_{34})JE^{-1}(S_{34}^T HS_{35} + S_{45})\}U\end{aligned} \tag{13}$$

The fellow Z_i of the eq.(13) can be replaced by the X_i using the constitutive low which describes the behaviour of the storage elements within the network $Z_i = F_i X_i$ with F_i a positive definite function. Using that, the eq.(13) is transformed as:

$$\begin{aligned}\dot{X}_i = \{(S_{11} - S_{13}HS_{13}^T) + (S_{14} + S_{13}HS_{34})JE^{-1}(S_{14}^T - S_{34}^T HS_{13}^T)\}F_i X_i + \\ \{(S_{15} + S_{13}HS_{35}) + (S_{14} + S_{13}HS_{34})JE^{-1}(S_{34}^T HS_{35} + S_{45})\}U\end{aligned} \tag{14}$$

The eq.(14) is a unique state space representation which, includes all the possible modes and proves that the extracted model is valid for both CCM and DCM.

4 Simulation Results

In this section the overall process will be implemented on two different topologies. For each, the Bond Graph models are developed and the differential equations are extracted. The behaviour of the models is described through their vector field diagrams, the mathematical models are implemented using MATLAB/SIMULINK and compared with the simulation of the converters using PSPICE. To aid direct comparison, the two programmes have been linked using the SLPS interface. This tool operates within the SIMULINK environment and the results of both simulators are extracted and displayed using MATLAB.

4.1 Boost Converter Example

The first topology presented is the Boost DC-DC converter Fig. 6. The values of the components have been chosen as: $E = 9\,Volts,\ L = 20\,\mu H,\ C = 20\,\mu F,\ R = 50\,\Omega$.

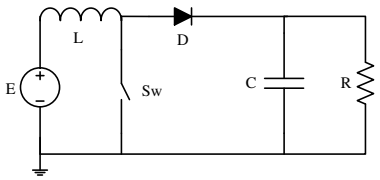

Figure 6: The circuit diagram of Boost Converter

The extracted Bond Graph model is shown in Fig. 7. The resistor R_{on} has been chosen as $R_{on} = 0.001\,\Omega$. For the diode, the resistor $R_d = 0.001\,\Omega$ is combined with the modulated transformer with m_2 modulation index. The modulation index m_2 takes binary values according to eq.(2) where $\Delta e = e_1 - e_2 - e_{11}$ and $e_{set} = 0$. The eq.(15) defines the resulting if-then rule that controls the diode.

$$m_2 = \begin{cases} 1 & if \quad E - L\frac{dI_L}{dt} - V_{out} \geq 0 \\ \\ 0 & if \quad E - L\frac{dI_L}{dt} - V_{out} < 0 \end{cases} \tag{15}$$

The additional resistor $R_{ad} = 1000\,Ohms$ has been placed to solve the causality conflict occurring at the 0-junction in which it participates. Since this resistor is placed in parallel with the switch, its value is required to be high in order not to affect the operation of the switch.

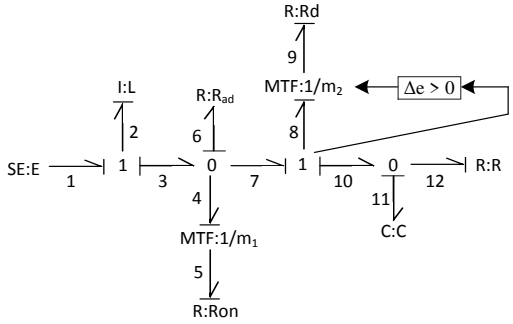

Figure 7: The Bond graph diagram of a Boost Converter

The mathematical model of the eq.(16) is obtained from the Bond Graph model, Figure 7 through a *"Sicuential Causality Assignment Procedure"* (SCAP) (Karnopp et al. 1990)

$$\left[\begin{array}{c} \dot{p}_2 \\ \dot{q}_{11} \\ \hline f_6 \\ e_{12} \\ \hline e_5 \\ e_9 \end{array}\right] = \left[\begin{array}{cc|cc|cc|c} 0 & 0 & -1 & 0 & 0 & 0 & 1 \\ 0 & 0 & 0 & -1 & 0 & m_2 & 0 \\ \hline 1 & 0 & 0 & 0 & -m_1 & -m_2 & 0 \\ 0 & 1 & 0 & 0 & 0 & 0 & 0 \\ \hline 0 & 0 & m_1 & 0 & 0 & 0 & 0 \\ 0 & -m_2 & m_2 & 0 & 0 & 0 & 0 \end{array}\right] \left[\begin{array}{c} f_2 \\ e_{11} \\ \hline e_6 \\ f_{12} \\ \hline f_5 \\ f_9 \\ \hline E \end{array}\right] \tag{16}$$

where $\dot{p_2}$ is the derivative of the momentum of the inertia element connected to bond 2 in Figure 7. This momentum is equal to: $p_2 = \int e_2 dt$ hence, $\dot{p_2} = e_2$. The $\dot{q}_{11}$ represents the displacement of the compliant element C which is connected with bond 11. The displacement can be expressed as: $q_{11} = \int f_{11} dt$ and so $\dot{q}_{11} = f_{11}$. The effort e_2 and the flow f_{11} represent the voltage across the inductor L and the current through

the capacitor C of the electric circuit in Figure 6. Hence the inductor's voltage is given by: $V_L = L\frac{dI_L}{dt}$ and the capacitor's current by: $I_C = C\frac{dV_{out}}{dt}$.

The implicit form is then derived as in eq.(17) after combining the eq.(4) with eq.(16):

$$\begin{bmatrix} \dot{X}_i \\ 0 \\ 0 \end{bmatrix} = \left[\begin{array}{cc|cc|cc|cc|cc|c} 0 & 0 & -1 & 0 & 0 & 0 & 0 & 0 & 0 & 0 & 1 \\ 0 & 0 & 0 & -1 & 0 & 0 & 0 & m_2 & 0 & 0 & 0 \\ \hline 1 & 0 & 0 & 0 & -1 & 0 & -m_1 & -m_2 & 0 & 0 & 0 \\ 0 & 1 & 0 & 0 & 0 & -1 & 0 & 0 & 0 & 0 & 0 \\ \hline 0 & 0 & -m_1 & 0 & 0 & 0 & 0 & 0 & -1 & 0 & 0 \\ 0 & m_2 & -m_2 & 0 & 0 & 0 & 0 & 0 & 0 & -1 & 0 \end{array}\right] W \tag{17}$$

The differential equations eq.(18) and eq.(19) are also provided below.

$$\begin{aligned} \frac{dI_L}{dt} = & -\frac{R_d R_{ad} R_{on}}{((R_{on} + m_1 R_{ad})R_d + R_{on} R_{ad} m_2)L} I_L \\ & - \frac{R_{ad} R_{on} m_2}{((R_{on} + m_1 R_{ad})R_d + R_{on} R_{ad} m_2)L} V_{out} + \frac{E}{L} \end{aligned} \tag{18}$$

$$\begin{aligned} \frac{dV_{out}}{dt} = & \frac{R_{on} R_{ad} m_2}{((R_{on} + m_1 R_{ad})R_d + R_{on} R_{ad} m_2)C} I_L \\ & - \frac{(R_{on} + m_1 R_{ad})(Rm_2 + R_d) + R_{on} R_{ad} m_2}{((R_{on} + m_1 R_{ad})R_d + R_{on} R_{ad} m_2)CR} V_{out} \end{aligned} \tag{19}$$

The evaluation and the behaviour of the mathematical model extracted for the Boost converter, is tracked via its vector field when the switch is ON, Figure 8 and OFF, Figure 9.

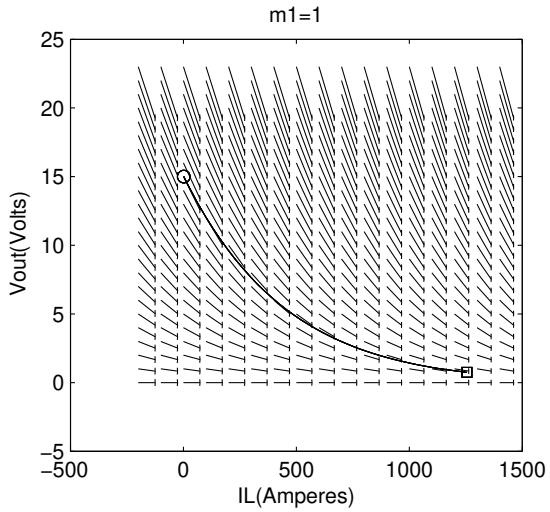

Figure 8: The vector field of a Boost Converter when its switch is ON while the diode is reversed

In Figure 9, the vectors starting from values $I_L < 0$ appear to have magnitude similar to the ones with value $I_L > 0$ due to normalisation. In reality, their magnitude is significantly higher than the rest of the field as both the switch and diode are disconnected in that area $m_1 = m_2 = 0$ while the inductor has some initial value. As a result, the inductor's derivative reaches a large value instantaneously ($\frac{dI_L}{dt} \to -\infty$), therefore even when the system starts its operation with negative initial conditions it will be forced to remain in the first quadrant of the vector field.

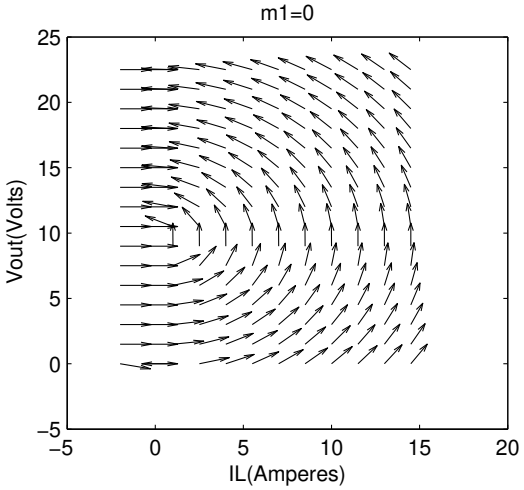

Figure 9: The vector field of a Boost Converter when its switch is OFF

The model described by eq.(18) and (19) is compared with a simulation of a boost converter using PSPICE. In Figure 10 the inductor current is demonstrated and Figure 11 shows the simulation results of the output voltage. A pulse signal with frequency $f = 100\,kHz$ drives the switch. During the simulation the converter operates in CCM where $E = 10\ Volts$ and the $V_{out} = 50\ Volts$. At $t_1 = 10\ msec$ the input voltage changes to $E = 36.5\ Volts$. In order for the output voltage to remain at $V_{out} = 50\ Volts$ the pulse width changes from 90% to 20% which forces the converter to operate in DCM for $t = 10\ msec$. At time $t_2 = 20\ msec$ the input voltage returns to $E = 10\,Volts$ and the pulse width to 90% and the system operates again in CCM.

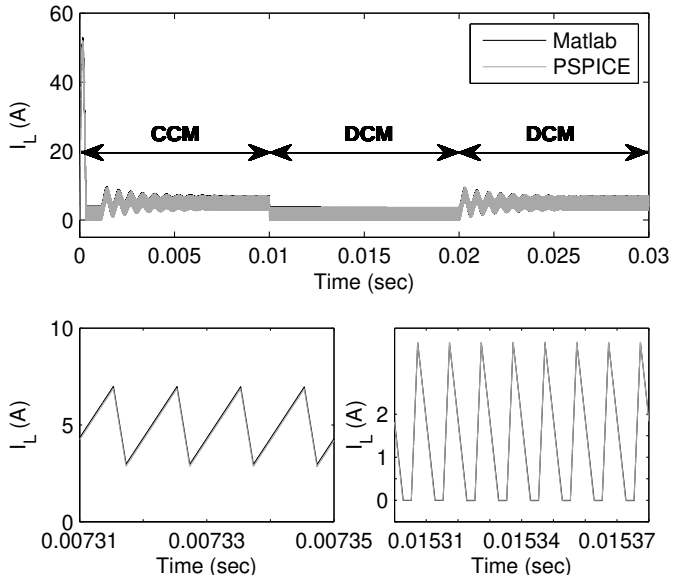

Figure 10: Comparing Inductor's current of a Boost Converter by simulating its operation using PSPICE (Grey Line) with the mathematical model as solved by matlab (Black). The converter operates in CCM for $t = 10\ msec$, passes to DCM until $t = 20\ ms$ and returns to CCM. Images below are zoomed areas for CCM and DCM from left to right

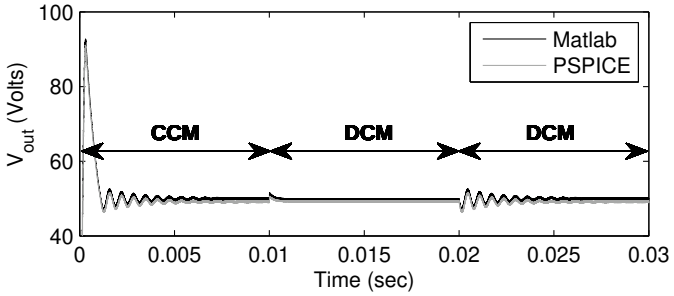

Figure 11: Comparing Output voltage of a Boost Converter by simulating its operation using PSPICE (Grey Line) with the mathematical model as solved by matlab (Black). The converter operates in CCM for $t = 10\ msec$, passes to DCM until $t = 20\ ms$ and returns to CCM

4.2 Buck Converter Example

For the Buck DC-DC converter, Figure 12, the values of components have been chosen as: $E = 9\,Volts, L = 50\,\mu H, C = 50\,\mu F, R = 30\,Ohms$.

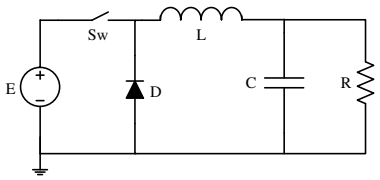

Figure 12: The circuit diagram of Buck Converter

The Bond Graph model of a Buck converter is presented in Figure 13. Similarly to the Boost converter Bond Graph Figure 7, the resistor $R_{ad} = 1\,k\Omega$ is added to resolve the causality conflict that occurs on the 0-junction it is connected to. The values of the resistors R_{on} and R_d have been chosen as: $R_{on} = 0.1\,m\Omega$, $R_d = 1\,m\Omega$. The corresponding to the diode modulation index m_2 is governed by the sign ($\pm$) of

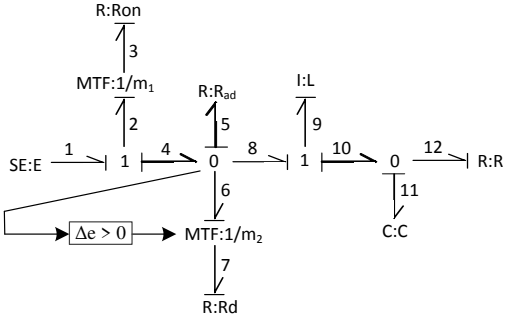

Figure 13: The Bond graph diagram of a Buck Converter

the effort e_5 across the 0-junction and is equal to: $e_5 = e_9 + e_{11}$. Therefore, the if-then rule governs the m_2 is given by eq.(20).

$$m_2 = \begin{cases} 1 & if \quad L\frac{dI_L}{dt} + V_{out} < 0 \\ \\ 0 & if \quad L\frac{dI_L}{dt} + V_{out} \geq 0 \end{cases} \tag{20}$$

The mathematical model of the Buck converter is given by eq.(21).

$$\left[\begin{array}{c} \dot{p}_9 \\ \dot{q}_{11} \\ \hline f_5 \\ e_{12} \\ \hline e_3 \\ e_7 \end{array}\right] = \left[\begin{array}{cc|cc|cc|c} 0 & -1 & 1 & 0 & 0 & 0 & 0 \\ 1 & 0 & 0 & -1 & 0 & 0 & 0 \\ \hline -1 & 0 & 0 & 0 & m_1 & -m_2 & 0 \\ 0 & 1 & 0 & 0 & 0 & 0 & 0 \\ \hline 0 & 0 & -m_1 & 0 & 0 & 0 & m_1 \\ 0 & 0 & m_2 & 0 & 0 & 0 & 0 \end{array}\right] \left[\begin{array}{c} f_9 \\ e_{11} \\ \hline e_5 \\ f_{12} \\ \hline f_3 \\ f_7 \\ \hline E \end{array}\right] \tag{21}$$

The implicit form is then as in eq.(22)

$$\left[\begin{array}{c} \dot{X}_i \\ 0 \\ 0 \end{array}\right] = \left[\begin{array}{cc|cc|cc|cc|cc|c} 0 & -1 & 1 & 0 & 0 & 0 & 0 & 0 & 0 & 0 & 0 \\ 1 & 0 & 0 & -1 & 0 & 0 & 0 & 0 & 0 & 0 & 0 \\ \hline -1 & 0 & 0 & 0 & -1 & 0 & m_1 & -m_2 & 0 & 0 & 0 \\ 0 & 1 & 0 & 0 & 0 & -1 & 0 & 0 & 0 & 0 & 0 \\ \hline 0 & 0 & m_1 & 0 & 0 & 0 & 0 & 0 & -1 & 0 & m_1 \\ 0 & 0 & -m_2 & 0 & 0 & 0 & 0 & 0 & 0 & -1 & 0 \end{array}\right] W \tag{22}$$

The differential equations for the inductor current I_L and the output voltage V_{out} are shown in eq.(23) and eq.(24).

$$\begin{aligned} \frac{dI_L}{dt} &= -\frac{R_{ad}R_{on}R_d}{((R_{on}+m_1R_{ad})R_d + R_{on}R_{ad}m_2)L} I_L \\ &\quad - \frac{1}{L}V_{out} + \frac{R_{ad}R_d m_1}{((R_{on}+m_1R_{ad})R_d + R_{on}R_{ad}m_2)L} E \end{aligned} \tag{23}$$

$$\frac{dV_{out}}{dt} = \frac{1}{C}I_L - \frac{1}{RC}V_{out} \tag{24}$$

The behaviour of the Buck converter's mathematical model is observed through the vector fields shown in Figure 14 when the switch is ON and Figure 15 when the switch is OFF. The vector field Figure 15 shows

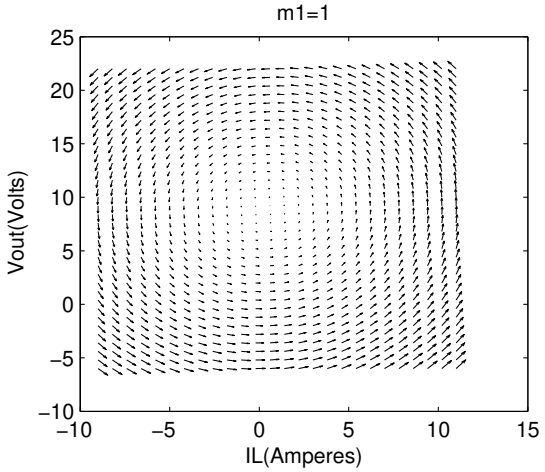

Figure 14: The vector field of a Buck Converter when its switch is ON while the diode is reversed

that the trajectories are restricted to remain within the first quadrant. The system is bounded by the lines $I_L = 0$ and $V_{out} = 0$ due to the operation of the diode. The vectors are also normalised as for the Boost Converter.

The model of eq.(23),(24) is compared with the simulation of the converter by PSPICE. In Figure 16 the inductor current of the converter is exhibited and Figure 17 shows the simulation results of the output

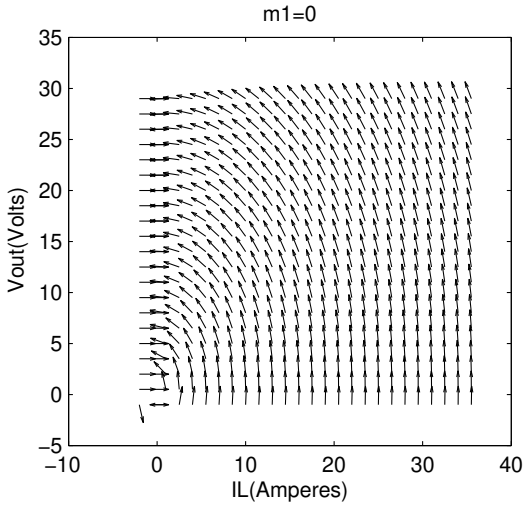

Figure 15: The vector field of a Buck Converter when its switch is OFF

voltage, which remains the same during the transition from CCM to DCM $V_{out} = 18Volts$. The switching frequency is again $f = 100kHz$, the input voltage in CCM $E = 20Volts$ and the pulse width is 80%. While in DCM, the input voltage is $E = 62Volts$ and the pulse width is 20%

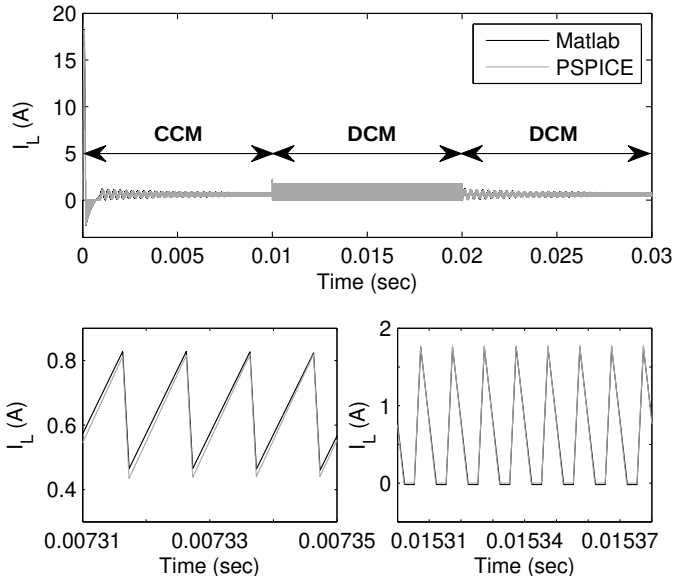

Figure 16: Comparing Inductor's current of a Buck Converter by simulating its operation using PSPICE (Grey Line) with the mathematical model as solved by matlab (Black). The converter operates in CCM for $t = 10\ msec$, passes to DCM until $t = 20\ ms$ and returns to CCM. Below images are zoom areas for CCM and DCM from left to right

In Figure 16 the current is allowed to reverse when the system is in its transient response due to the output voltage being greater than the input during this time interval.

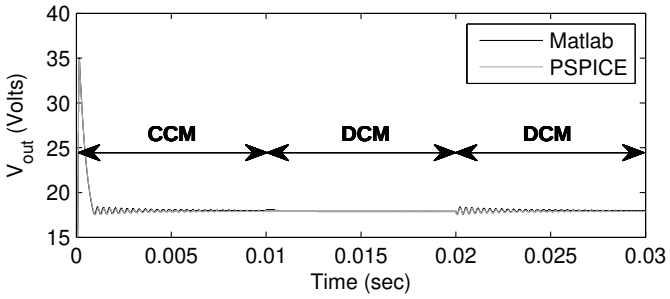

Figure 17: Comparing Output voltage of a Buck Converter by simulating its operation using PSPICE (Grey Line) with the mathematical model as solved by matlab (Black). The converter operates in CCM for $t = 10\ msec$, passes to DCM until $t = 20\ ms$ and returns to CCM

5 Experimental Results

To verify the validity of the model against a real practical system, the BuckBoost Converter PICtail Plus Daughter Board developed by Microchip, has been employed. This Daughter Board contains three converters: two Buck and one Boost. In the practical implementation, one of the Buck Converters is operated in both CCM and DCM to facilitate a comparison with the simulation results. The buck converter operates in CCM when an external resistive load of $R = 5\ Ohms$ is connected, and the converter operates in DCM when the resistive load is $R = 38\ Ohms$.

The Daughter Board contains a current sensor connected to the FET switch of the converter, rather than directly to the inductor. Therefore, the inductor current is captured only for the time period when the switch is ON. When the switch goes OFF the sensing current goes to zero. When the switch turns ON again, if the converter operates in CCM, the Current instantaneously reaches a value as shown in Figure 18. During DCM the current starts from zero and ramps up until the switch turns OFF, as shown in Figure 19.

Moreover, an offset in the inductor current $I_{offset} = 0.45\ A$ is observed in both Figures 18,19. This offset has been designed by the manufacturer to facilitate the Analogue to Digital conversion, with value corresponding to $I_L = 0.45\ A$ rather than $I_L = 0\ A$. The current produced by the model I_L is adjusted to follow this offset, and the accuracy is increased by choosing appropriate values for the resistors $R_{on} = R_d = 0.7\ Ohms$.

The switching pulse is generated by a Microchip dsPIC33FJ256GP710A mounted on a Microchip Explorer 16 Development Board. The switching frequency is chosen as $f = 400\ kHz$ while the Pulse width is 50% for both CCM and DCM.

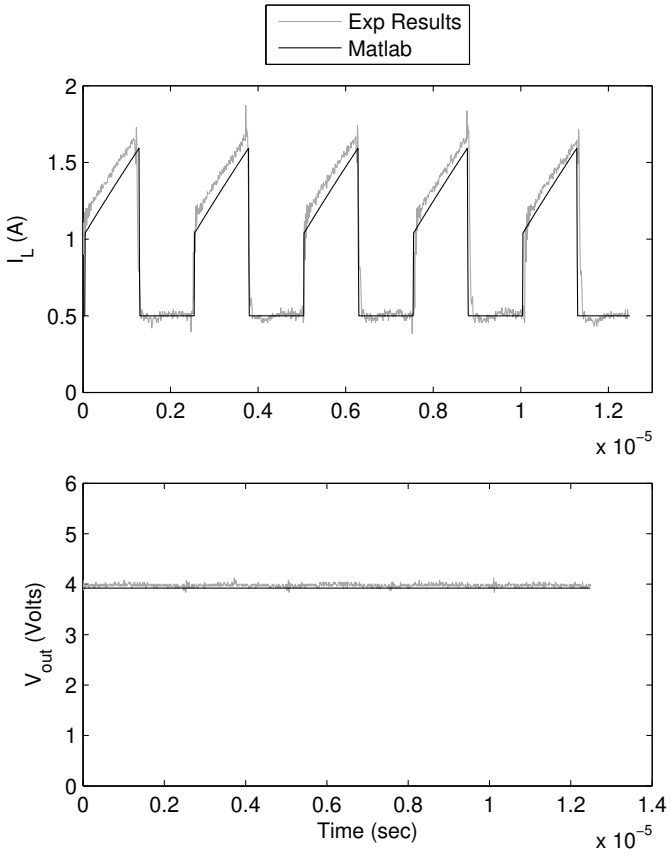

Figure 18: Inductor current and output voltage of a Buck converter operating in CCM

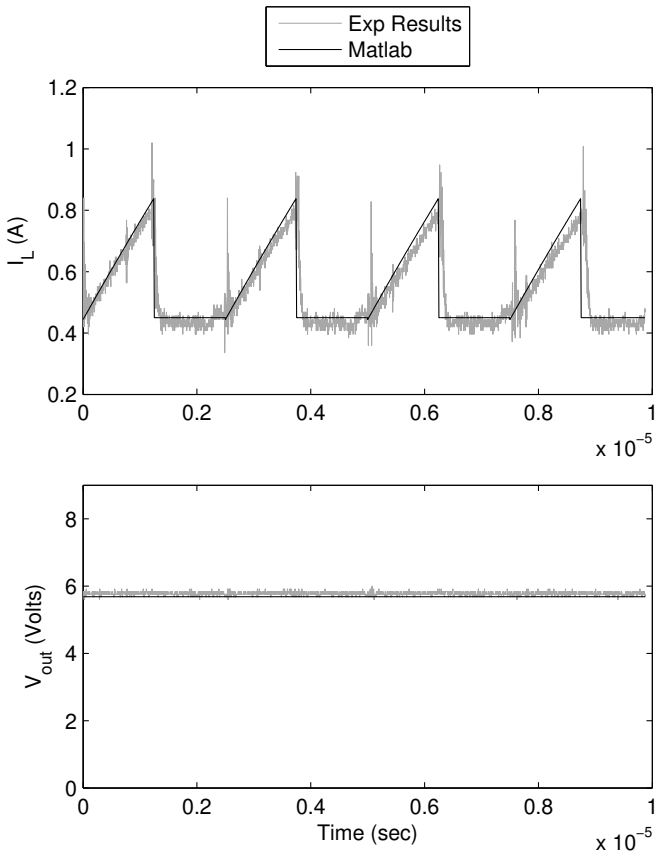

Figure 19: Inductor current and output voltage of a Buck converter operating in DCM

6 Discussion on the Results

The simulation results of the two previous examples appear to have high accuracy. The models extracted from the Bond Graphs in each case follow the simulation of the converters using PSPICE accurately even through the transitions of the converter from CCM to DCM. The vector fields reveal that the model is accurate in a wide range of initial conditions. Furthermore, the mathematical model has adequate performance with variable switching frequency, load and input voltage. The vector fields also reveal that the equilibrium is a neighbourhood, due to the ac component inherent in the output voltage. This results in a ripple in the output voltage.

The overshoot appearing in Figures 10, 11, 16, 17, is due to uncharged output capacitors and lasts only for few *usecs* and happens only at the beginning of the simulation. Moreover, an ideal model produces more overshoot than a system containing physical components with *"Equivalent Series Resistances"*(ESRs) which result in lower overshoot.

The error between the mathematical models extracted from the Bond Graphs and implemented by MATLAB, and the simulation of the converters using PSPICE is evaluated by calculating the Normalised Root Means Square Error (NRMSE). The NRMSE is defined in eq.(25):

$$NRMSE = \frac{\sqrt{\frac{1}{N}\sum_{i=1}^{N}(x_i - y_i)^2}}{y_{max} - y_{min}} \tag{25}$$

where N is the number of samples captured by SLPS/Simulink and extracted in MATLAB. This number varies for each case while the step size has been chosen to be fixed at $T_s = 10^{-8}$. Also, x_i is the i^{th} value of the state variables generated in each i sample while y_i is the i^{th} value of the state variables generated by PSPICE.

To ensure there are no spikes or Dirac pulses in the error calculations, the Maximum Absolute Error (MAE) has also been calculated as in eq.(26).

$$MAE = \max_{1 \le i \le N} \mid x_i - y_i \mid \tag{26}$$

The results extracted from eq.(25) and eq.(26) are provided in the (Table 1) below, where both NRMSE and MAE are increased when high overshoot occurs. This is due to high rate of change in each time constant when the converter is in transient, whereas in steady state the values of both errors are not significantly increased. Additionally, in DCM the NRMSE is higher compared to CCM.

Table 1: Results Produced by Normalised Root Mean Square Error

	CCM		DCM	
	NRMSE	Max Error	NRMSE	Max Error
BOOST I_L	0.0037	0.9854	0.0070	0.1367
BOOST V_{out}	0.0099	1.6676	0.4104	0.9114
BUCK I_L	0.0029	2.6986	0.0127	0.0892
BUCK V_{out}	0.0029	0.2845	0.1903	0.0808

Differences between the mathematical model and the PSPICE simulations occurred mainly due to the representation of the diode and the necessity of small constant step-times due to stiff equations. The representation of the diode using the MTF-R method results in linear instead of curved characteristic, Figure 3. However, PSPISE uses components with characteristics similar to the real ones. This difference leads to the voltage drop to be different between the two models. Moreover, the representation of the diode by the MTF-R is not capable of representing the voltage drop of a real component when it conducts, which typically is $V_d \simeq 0.8\, Volts$.

Small constant times are needed due to the extracted differential equations, which are stiff when they are solved by specific numerical solvers. The stiffness phenomenon, studied by Dijk & Breedveld (1991*a*,*b*),

occurs because the values of the resistors R_{on}, R_d are very small and appear in the denominator of the differential equations (Borutzky 1995). The way for this phenomenon to be avoided is to decrease the step size significantly (max step size $\geq 10^{-7}$) although memory problems and long simulation time may become an issue. Nevertheless, these small differences between the model and the actual converter can be evaluated and any impact mitigated through using appropriate control.

7 Conclusion

In this paper, a mathematical model for conventional DC-DC converters with one switch and one diode has been extracted via Bond Graphs such that the new model can operate in both CCM and DCM and also allow for independent operation of the switch and diode. The operation of a switch is represented by a combination of modulated transformers MTF with binary modulation index and resistors, called the MTF-R method.

The MTF-R method leads to fixed causality models which remain the same during commutation. Furthermore, utilisation of this method allows the switches participating in the system to operate independently without any correlation between them. Moreover, the MTF-R method allows a direct binary control input to be implemented unlike averaged models. Causality conflict arises while the diode and the switch are connected between them and is solved by using one additional resistive element connected in parallel with the switch. This resistor's value needs to be so high as not to affect the operation of the switch.

The operation of the diode has been represented through the MTF-R method by using an internal control loop that governs the modulation of the MTF according to the difference of the effort (voltage) in the junction where it participates.

The mathematical model, valid for both CCM and DCM, has been extracted from the Bond Graphs using standard SCAP without any modifications. The implicit equation and a unique state space equation of this mathematical model have been derived with all of the operation modes to be proven valid. The operation of the model capable of representing both CCM and DCM has also been demonstrated through an automaton diagram.

The new modelling method has been implemented in two different converter topologies, Buck and Boost, and their behaviour is evaluated through their vector fields. Numerical results, obtained by MATLAB/SIMULINK, have been compared with the simulation of the converters' operation using PSPICE. The differences between the new model and the PSPICE simulation results are evaluated through the Normalised Root Mean Square Error and the Maximum Absolute Error and overall the new model performs very well. Experimental results are also provided with the model tested on a Buck Converter topology, for both CCM and DCM. The results show adequate accuracy.

References

Borutzky, W. (1995), 'Discontinuities in a bond graph framework', *Journal of the Franklin Institute* **332**(2), 141–154.

Borutzky, W. (2010), *Bond Graph Methodology : development and analysis of multidisciplinary dynamic system models*, Springer, London.

Borutzky, W. (2012), 'Bond-graph-based fault detection and Isolation for hybrid system models', *Systems and Control Engineering* **226**(6), 742–760.

Buisson, J. (1993), Analysis and characterisation of hybrid systems with bond-graphs, *in* 'Proceedings Systems Man and Cybernetics Conference SMC', IEEE, pp. 264–269.

Buisson, J. (2001), Bond graph modeling of power converters with switches commutating by pairs, *in* 'Proceedings Conference on Bond Graph Modeling and Simulation (ICBGM)', SCS Publishing, pp. 2–7.

Buisson, J., Cormerais, H. & Richard, P.-Y. (2002), 'Analysis of the bond graph model of hybrid physical systems with ideal switches', *Journal of Systems and Control Engineering* **216**(1), 47–63.

Cormerais, H. & Buisson, J. (2000), A mathematical criteria to determine the valid modes of a hybrid system, *in* 'IFAC Symposium on Power Plants & Power Systems Control, Brussels'.

Dauphin-Tanguy, G. & Rombaut, C. (1993), Why a unique causality in the elementary commutation cell bond graph model of a power electronics converter, *in* 'Proceedings of IEEE Systems Man and Cybernetics Conference - SMC', IEEE, pp. 257–263.

Dijk, J. V. & Breedveld, P. (1991*a*), 'Simulation of system models containing zero-order causal paths–I. Classification of zero-order causal paths', *Journal of the Franklin Institute* pp. 959–979.

Dijk, J. V. & Breedveld, P. (1991*b*), 'Simulation of system models containing zero-order causal paths–II Numerical implications of class 1 zero-order causal paths', *Journal of the Franklin Institute* pp. 981–1004.

Ducreux, J., Dauphin-Tanguy, G. & Rombaut, C. (1993), Bond Graph Modelling of Commutation Phenomena in Power Electronics Circuit, *in* 'Proceedings International Conference on Bond Graph Modelling (ICBGM)', Western Simulation Multiconference, pp. 132–136.

Femia, N. & Tucci, V. (1994), 'On the modeling of pwm converters for large signal analysis in discontinuous conduction mode', *IEEE Transactions on Power Electronics* **9**(5), 487–496.

Huber, L., Irving, B. & Jovanovic, M. (2008), 'Open-loop control methods for interleaved DCM/CCM boundary boost PFC converters', *IEEE Transactions on Power Electronics* **23**(4), 1649–1657.

Karnopp, D., Margolis, D. L. & Rosenberg, R. C. (1990), *System Dynamics: A Unified Approach*, 2nd edn, WileyInterscience, New York.

Lai, J.-S. & Chen, D. (1993), Design consideration for power factor correction boost converter operating at the boundary of continuous conduction mode and discontinuous conduction mode, *in* 'Proceedings Eighth Annual Applied Power Electronics Conference and Exposition,', IEEE, pp. 267–273.

Markakis, A., Holderbaum, W. & Potter, B. (2011), A comparison between bond graphs switching modelling techniques implemented on a boost dc-dc converter, *in* 'Proceedings International Telecommunications Energy Conference (INTELEC)', IEEE, pp. 1–7.

Mirzaei, M. & Afzalian, A. A. (2009), 'Hybrid modelling and control of a synchronous dc-dc converter', *International Journal of Power Electronics* **1**(4), 414–433.

Mosterman, P. J. & Biswas, G. (1998), 'A theory of discontinuities in physical system models', *Journal of the Franklin Institute* **335**(3), 401–439.

Paul, A. K. (2013), 'Practical inputs for maturity model of sliding mode control concepts in power electronics domain', *International Journal of Power Electronics* **5**(2), 145–164.

Paynter, H. M. & Briggs, P. (1961), *Analysis and design of engineering systems*, M.I.T. Press, Cambridge, MA.

Rai, U. B. & Umanand, L. (2009), 'Generalised bond graph model of a rotating machine', *International Journal of Power Electronics* **1**(4), 397–413.

Umarikar, A. C. & Umanand, L. (2005*a*), Modelling of switched mode power converters using bond graph, *in* 'Electric Power Applications, Iee Proceedings-', Vol. 152, IET, pp. 51–60.

Umarikar, A. & Umanand, L. (2005*b*), 'Modelling of switching systems in bond graphs using the concept of switched power junctions', *Journal of the Franklin Institute* **342**(2), 131–147.

Vorperian, V. (1990*a*), 'Simplified analysis of PWM converters using model of PWM switch. II. Discontinuous conduction mode', *IEEE Transactions on Aerospace and Electronic Systems* **26**(3), 497–505.

Vorperian, V. (1990*b*), 'Simplified Analysis of PWM Converters Using Model of PWM Switch Part I: Continuous Conduction Mode', *IEEE Transactions on Aerospace and Electronic Systems* **26**(3), 490–496.